We are IntechOpen,
the world's leading publisher of
Open Access books
Built by scientists, for scientists

6,900
Open access books available

185,000
International authors and editors

200M
Downloads

154
Countries delivered to

Our authors are among the

TOP 1%
most cited scientists

12.2%
Contributors from top 500 universities

CLARIVATE ANALYTICS

BOOK CITATION INDEX

INDEXED

WEB OF SCIENCE™

Selection of our books indexed in the Book Citation Index
in Web of Science™ Core Collection (BKCI)

Interested in publishing with us?
Contact book.department@intechopen.com

Numbers displayed above are based on latest data collected.
For more information visit www.intechopen.com

Application of Optical Interferometry for Characterization of Thin-Film Adhesion

Sanichiro Yoshida , David R. Didie ,
Jong-Sung Kim and Ik-Keun Park

Additional information is available at the end of the chapter

Abstract

In this chapter, application of optical interferometry for the characterization of thin-film adhesion to the substrate is discussed. The thin-film system is configured as one of the end mirrors of a Michelson interferometer and oscillated with an acoustic transducer from the substrate side. The oscillation causes sinusoidal displacement of the film surface around the initial (neutral) position, and the interferometer detects its amplitude as the relative phase difference behind the beam splitter. When the driving frequency of this oscillation is tuned to a range where the film-substrate interface is dominantly oscillated, the elasticity of the interface can be analyzed from the oscillation amplitude. The principle of this method is straightforward but in reality, fluctuation of the initial phase (the relative phase corresponding to the initial film position) compromises the signal. A technique known as the carrier fringe method along with spatial frequency domain analysis is employed to reduce the noise associated with the initial phase fluctuation. The possibility of the present method to analyze the so-called blister effect on thin-film adhesion is discussed.

Keywords: optical interferometry, opto-acoustic technique, thin-film adhesion, blister effects, non-destructive evaluation

1. Introduction

Thin-film systems are used in a variety of applications ranging from micro-electro-mechanical-systems (MEMS) to artificial joints. Poor adhesion of the film material to the substrate leads to delamination or other modes of coating failure, and is an important factor of quality control in

the manufacturing stage. However, detection of poor adhesion is not easy. In particular, when the film material is poorly adhered but not causing a structural abnormality, detection is very difficult. Static methods such as acoustic imaging microscopy or X-ray diffractometry cannot be used to identify the problem. Dynamic analysis capable of characterizing the elastic behavior of the interface is essential.

Among dynamic techniques to evaluate the film adhesion strength, ultrasonic techniques [1–5] are the prevailing methods. In these methods, ultrasonic waves are excited in the substrate and film materials, and abnormality is detected from the propagation characteristics of the ultrasonic wave. The recent trend indicates that the film thickness is reduced for better performance of the thin-film system. This forces the ultrasonic wavelength to be shorter, hence the frequency to be higher. Reduction in the wavelength works well for the purpose of detecting defects or other nonuniform issues in the interface, as the spatial resolution is increased. However, for characterization of elasticity of the film-substrate interface, an increase in the frequency makes the analysis difficult. This is because normally, poor adhesion has lower elastic modulus than the healthy adhesion. Consequently, the frequency is too high to oscillate the poor adhesion effectively, and the signal representing the poor adhesion tends to be small. In other words, the detection system tries to probe the oscillatory behavior caused by the poor adhesion at a frequency on the blue side of the spectrum, as schematically illustrated in **Figure 1**. The transmissibility (the transfer function) of a mechanical oscillator decreases with a quadratic dependence on the frequency (f^{-2}) on the high frequency side of the resonance.
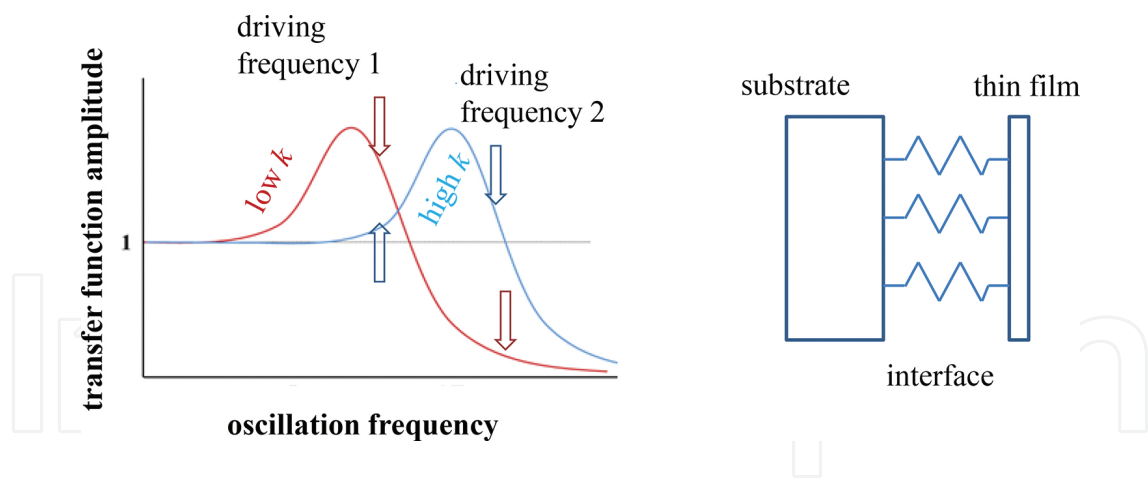
Figure 1. Resonance curves with different resonant frequencies.

Considering the above situation, we have devised an optical interferometric system to characterize the adhesion of thin films to their substrate [6]. A Michelson interferometer is used to analyze harmonic response of thin-film specimens when they are oscillated with an acoustic transducer. The film surface displacement resulting from the acoustic oscillation is detected as relative optical path changes behind the beam splitter. With the assumption that the film-substrate interface has a lower elastic modulus than the film or the substrate material and by choosing the acoustic frequency appropriately, it is possible to characterize the elastic behavior

of the interfaces. For several thin-film specimens, resonance-like behaviors of the film-substrate interface have been found [7].

In the course of this research, we have learned much about practical issues of Michelson interferometers. The operation principle of a Michelson interferometer is straightforward. However, in reality, its application to engineering is not as simple as it sounds. Especially, when the interferometer is used in air, environmental disturbance can easily affect the measurement. It is always possible to place the entire interferometric paths in a vacuum, but it causes extra costs and handling procedures. In many engineering applications, it is not favorable.

In this paper, after various findings from the above research being discussed, a method is proposed to reduce environmental disturbance that compromises the optical phase signal representing the oscillation at the acoustic frequency. In this method, a known optical-path variation is introduced in a direction lateral to the interferometer axis so that the Initial Phase Difference is visualized as a pattern of mutually parallel dark and bright stripes (known as a carrier-fringe pattern [8]), and the data is processed in the spatial-frequency domain. With this configuration, a change in the relative optical path shifts the fringe locations in a plane normal to the interferometric axis. This allows us to perform two-dimensional analysis on the image plane of the imaging device, and thereby find a weakly-adhered spot. The method is especially useful when the frame rate of the imaging device is significantly lower than the acoustic frequency, as is normally in this case. Under this condition, the relative phase change at the acoustic frequency is detected as the corresponding reduction in the fringe contrast that can be related to the height of the main peak in the Fourier spectrum. Since the spatial frequency corresponding to the main peak is determined by the spacing of the carrier fringe pattern, the peak value does not depend on slow shift of the entire fringe pattern due to an environmental disturbance.

2. Michelson interferometer for thin film analysis
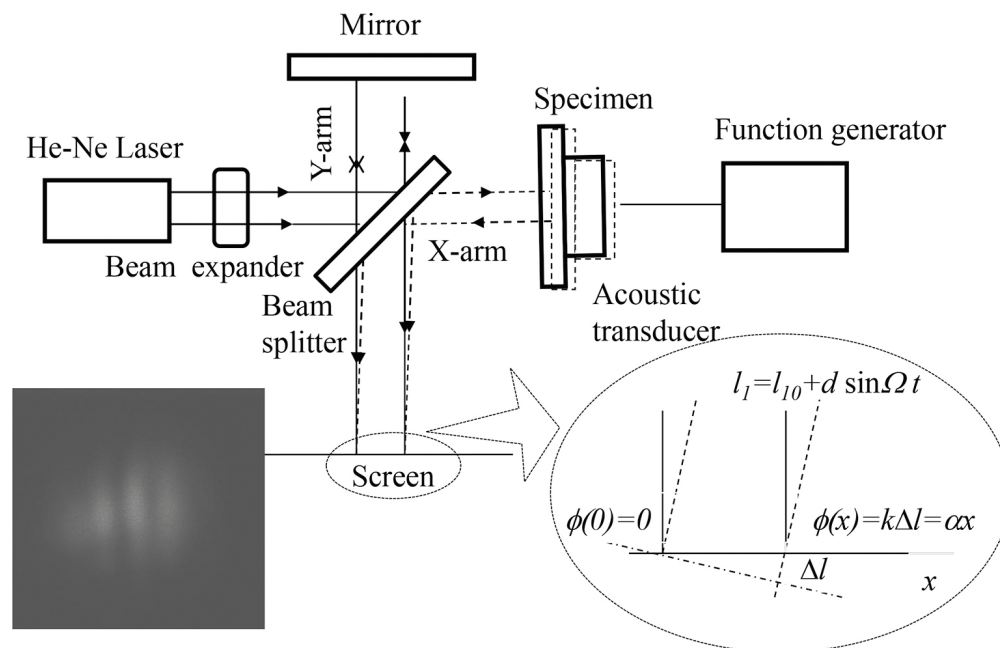
2.1. Why optical interferometer?

The substrate of typical thin film systems is of the order of 100 μm or less in thickness. In order to excite 10 waves in the substrate, the wavelength of the acoustic signal must be 10 μm or shorter. The acoustic velocity in silicon (a typical substrate) is 8 km/s. This results in the acoustic frequency higher than 800 MHz, leading to the situation where detection of elastic behavior associated with resonant frequency of the order of 100 MHz or less is difficult. Poor adhesion normally has a resonant frequency substantially lower than 100 MHz. In addition, most thin-film systems are subject to environmental disturbance of much lower frequency. Therefore, the use of high acoustic frequency is unrealistic.

2.2. Optical configurations

Figure 2 illustrates the principle of operation of the present method. A Michelson interferometer is configured with one end mirror replaced by the thin-film specimen. Call this interfero-

metric arm the signal arm, and the other the reference arm. In the signal arm, the specimen is placed with the film side facing the beam splitter. The specimen is oscillated with an acoustic transducer from the rear (substrate) side, and the resultant oscillation of the film surface is detected as the corresponding change in the optical path length relative to the reference path. It is postulated that the elastic modulus of the interface is lower than that of the film or the substrate material, as the right drawing of **Figure 1** illustrates. With this postulate, it follows that the resonant frequency of the interface is lower than that of the film or substrate. In other words, when the acoustic frequency is tuned in a frequency range where the interface can possibly have resonant points, both the film and substrate oscillate as rigid bodies. Therefore, it is possible to detect the differential displacement of the film surface that represents the dynamics of the interface.

Figure 2. Michelson interferometer and experimental arrangement.

2.3. Optical intensity behind beam splitter

The light intensity on the image plane behind the beam splitter can be expressed as follows.

$$I(t) = 2I_0 + 2I_0 \cos\left[k\left(l_{s0} - l_{r0}\right) + kd\sin\omega t\right] = 2I_0 + 2I_0 \cos\left[\delta_0 + \delta\sin\omega t\right] \quad (1)$$

Here I_0 is the intensity of the reference and signal beams, k is the wave number of the laser light in (rad/m), l_{s0} and l_{r0} are respectively, the initial (physical) length of the signal and reference arms, $\delta_0 = l_{s0} - l_{r0}$ is the arm length difference, $\delta = kd$ and d are the oscillation amplitude of the film surface in (rad) and (m), and ω is the oscillation (driving) angular frequency of the film specimen. Here the reference and signal beams are the noninterfering light beams in the

reference and signal arms, respectively; their intensities are assumed to be equal to each other. (In reality, they are not equal to each other but the gist of the argument here is not affected by inequality. The error associated with the inequality is discussed later in this paper.) The second term in the right-hand side of Eq. (1) with $\cos[\delta_0 + \delta \sin \omega t]$ is called the interference term. This term is important as it contains the relative phase change information. $I(t)$ is captured by a photodetector or an imaging device placed behind the beam splitter.

Two methods are possible to detect the relative optical path change behind the beam splitter. Call them the total-intensity and two-dimensional methods. Both methods have advantages and disadvantages. In the total-intensity method, the total intensity $I(t)$ is captured by a fast photodetector such as a silicon PIN photodiode. The advantage of this method is that the response time of the detector is fast enough to analyze $I(t)$ at the same frequency as the acoustic transducer (ω in Eq. (1)). A disadvantage of this method is that it detects the interference term representing the entire cross-sectional area of the laser beam reflected off the specimen. It is unable to resolve the intensity over the plane of the specimen. Another disadvantage of this method is that it is vulnerable to unwanted optical path changes due to environmental disturbance.

In the two-dimensional method, an imaging device (an array of photodetector such as a CCD (Charge Coupled Device)) is used for the photodetector behind the beam splitter. (Hereafter, this type of imaging device is referred to as a CCD.) A typical CCD consists of approximately 500 rows and 500 columns of pixels. It is possible to detect the relative phase change two dimensionally on a pixel-by-pixel basis. Another advantage of this method is that by intro-ducing a so-called carrier fringe system, it is possible to reduce the influence of the unwanted optical path length change due to environmental disturbance. The disadvantage of this method is that the frame rate (the sampling rate) of a CCD has normally orders of magnitude lower than the acoustic frequency. Consequently, the detected signal is greatly down-sampled. Below we discuss the two configurations in more detail.

2.3.1. Total intensity configuration

In this configuration, the light beams from the two arms are aligned so that they overlap each other for the entire path they share, i.e., the optical path from the beam splitter to the photo-detector. Under these conditions, the film surface displacement due to the acoustic oscillation changes the relative path length difference commonly to all points on the x-y plane (the plane of the specimen). The photodetector signal is proportional to the total intensity expressed by Eq. (1), where the oscillation comes from the interference term. By measuring the intensity of the signal beam and the reference beam separately, we can evaluate $2I_0$ and express the interference as follows.

$$\cos\left[\delta_0 + \delta \sin \omega t\right] = \frac{I(t) - 2I_0}{2I_0} \tag{2}$$

In evaluating the oscillation amplitude δ from Eq. (2), the initial phase difference δ_0 plays an important role. The phase oscillation due to the acoustic transducer occurs around δ_0. Since the function $\cos\theta$ has the greatest slope at $\theta = 0$, the oscillation amplitude of Eq. (2) is maximized when $\delta_0 = 0$. In other words, the amplitude of the oscillation due to δ is maximized when the initial interference is totally destructive. **Figure 3** illustrates this situation for $\delta_0 = 0, \ \frac{\pi}{4}, \ \frac{\pi}{2}$, when the oscillation amplitude δ is 0.2 as an example. The issue is that when an environmental factor such as changes in the refractive index of the air due to temperature fluctuations vary the value of δ_0 in a random fashion, it becomes impossible to distinguish whether observed interferometric intensity variation is due to δ or δ_0 in Eq. (2).
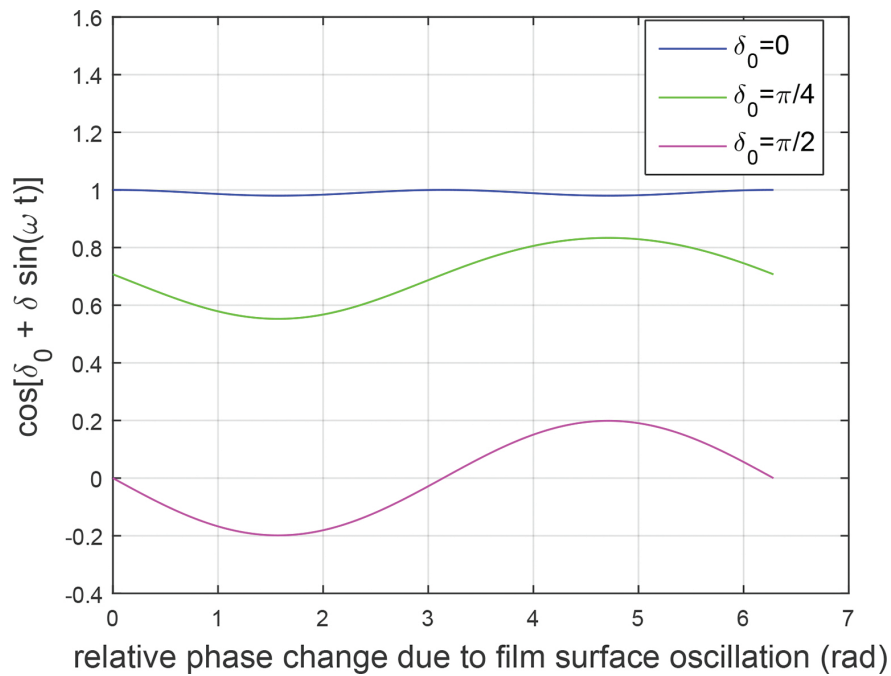
Figure 3. Interference term with three different initial phases.

2.3.2. Two-dimensional configuration

In this configuration, a CCD is used to capture the intensity represented by Eq. (1). Normally, the frame rate of a CCD is significantly lower than the acoustic frequency. A CCD with a frame rate comparable to the acoustic frequency is available but it is expensive and sometimes the number of pixels is limited in exchange for a higher frame rate. So, here we discuss image analysis for a low frame rate case.

The issue of environmental relative phase fluctuation discussed above applies to the two-dimensional configuration as well. However, the introduction of a carrier fringe system in conjunction with frequency domain analysis greatly overcomes this issue. Below we first consider the case when a carrier fringe system is not introduced (called the simple Michelson method) followed by the carrier fringe method.

(a) Simple Michelson method

Eq. (1) represents the instantaneous intensity observed behind the beam splitter. To discuss the case where the CCD's frame rate is much lower than the signal frequency, it is convenient to rewrite Eq. (1) in terms of Bessel functions of first kind. Using the following identities,

$$\cos\left(\delta\sin\omega t\right) = J_0\left(\delta\right) + 2J_2\left(\delta\right)\cos 2\omega t + 2J_4\left(\delta\right)\cos 4\omega t + \cdots$$

$$\sin\left(\delta\sin\omega t\right) = 2J_1\left(\delta\right)\sin\omega t + 2J_3\left(\delta\right)\sin 3\omega t + \cdots$$

Eq. (1) can be rewritten as follows.

$$
\begin{aligned}
I\left(t\right) &= 2I_0 + 2I_0\cos\left(\delta_0 + \delta\sin\omega t\right) = 2I_0 + 2I_0\cos\delta_0\cos\left(\delta\sin\omega t\right) - \\
&2I_0\sin\delta_0\sin\left(\delta\sin\omega t\right) = 2I_0 + 2I_0\cos\delta_0\left\{J_0\left(\delta\right) + 2J_2\left(\delta\right)\cos 2\omega t\right\} + \\
&2J_4\left(\delta\right)\cos 4\omega t + \cdots\} - 2I_0\sin\delta_0\{2J_1\left(\delta\right)\sin\omega t + 2J_3\left(\delta\right)\sin 3\omega t + \cdots\}
\end{aligned}
\tag{3}
$$

In the present case, the acoustic frequency is in the range of 1–20 KHz, and the CCD has a frame rate of 30 fps (frames per second), or three orders of magnitude lower than the acoustic frequency. In other words, the data taken by the digital camera is greatly down-sampled. Under these conditions, the output of the CCD $S(\tau) = \int_0^\tau I(t)dt$ can be expressed as follows.

$$
\begin{aligned}
&2I_0\int_0^\tau\left\{1 + \cos\delta_0 J_0\left(\delta\right)\right\}dt + 4I_0\cos\delta_0\sum_{N=1}^\infty\int_0^\tau J_{2N}\left(\delta\right)\cos\left(2N\omega t\right)dt - \\
&4I_0\sin\delta_0\sum_{N=1}^\infty\int_0^\tau J_{2N-1}\left(\delta\right)\sin(2N-1)\omega t
\end{aligned}
\tag{4}
$$

Here τ is the exposure time of the CCD and N is an integer. Of the terms on the right-hand side of Eq. (4), those terms that contain the summation over N oscillate. On the other hand, the first integral is constant with respect to time and therefore increases in proportion to τ. Consequently, under the condition where the exposure time is much greater than the period of oscillation, i.e., $\tau \gg 2\pi/\omega$, the signal $S(\tau)$ can be approximated by the first integral.

$$S\left(\tau\right) \cong 2I_0\tau\left\{1 + \cos\delta_0 J_0\left(\delta\right)\right\}\tag{5}$$

Figure 4 compares the signal evaluated by Eq. (4) and the approximate signal by Eq. (5) for the driving frequency of 11 KHz as a function of the exposure time. It is seen that for $\tau = 1/30 = 33$

(ms), the exposure time corresponding to the frame rate of 30 fps (the frame rate used in the present study), the approximation by Eq. (5) is accurate.
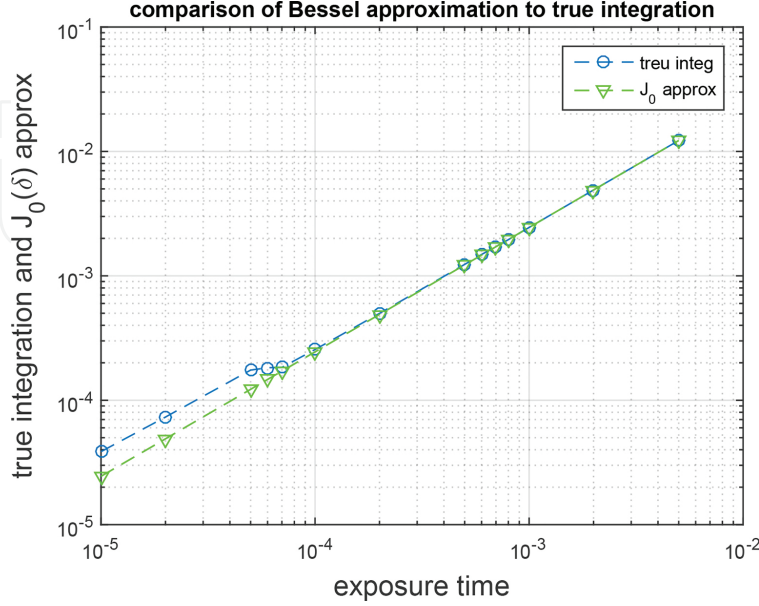
Figure 4. Comparison of $J_0(\delta)$ approximation and complete integral.

In Eq. (5), the first term $2I_0\tau$ is the sum of the optical intensity of the signal and reference arms. Experimentally, these intensities can be easily obtained by blocking one of the arms at a time and using the CCD behind the beam splitter. By subtracting this term from the total signal and dividing the result by $2I_0\tau$, we can derive expression of the interference term (Eq. (2)) for the total intensity configuration as follows.

$$\cos\delta_0 J_0(\delta) = \frac{S(\tau) - 2I_0\tau}{2I_0\tau} \tag{6}$$

In principle, by knowing the initial relative phase δ_0 from an independent experiment (such as changing the reference arm length through fringes with the acoustic transducer turned off), we can even estimate the value of δ from the known curve of $J_0(\delta)$ and $d = \delta/k$. However, in reality, environmental noise causes fluctuations in the optical path length. As will be discussed later, a temperature change of 0.1°C in the air in the beam path can cause a considerable change in the relative phase δ_0. Also, angular misalignment such as the one due to seismic disturbance reduces the accuracy in the subtraction of the I_0 in Eq. (6); since the intensity of the reference and signal beams is measured at different times from the total intensity, any angular misalignment shifts the beam center on the image plane of the CCD, and that reduces the accuracy of Eq. (6).

(b) Carrier fringe method

In this method a linear spatial phase-variation is introduced so that the relative phase changes over several periods of 2π across the cross-section of the laser beam. This technique is known as the introduction of carrier fringes and widely used in ESPI (Electronic Speckle–Pattern Interferometry) [7]. Carrier fringes can be introduced by slightly tilting the specimen or the reference mirror, or by inserting a mechanism to introduce a linear phase variation such as an optical wedge. **Figure 2** shows an example where the specimen is slightly tilted.

We can express the CCD's output in this case by replacing $\cos \delta_0$ with $\cos \alpha x$ as follows.

$$S(\tau) \cong 2I_0\tau\{1 + \cos\alpha x J_0(\delta)\} \tag{7}$$

Here, x is the coordinate axis set up on the specimen's surface and α is the angle of tilt.

The advantage of this technique in the present context is as follows. In the simple Michelson method, if environmental disturbance changes the relative phase, it directly affects the signal expressed by Eq. (5). There is no way of knowing whether the change in the signal is due to the oscillation amplitude or the environmental noise unless the sampling rate of the optical detector is higher than the acoustic frequency. When the sampling rate is lower than the acoustic frequency, the detector's signal passes though a number of maxima and minima corresponding to the constructive and destructive interference. On the other hand, if carrier fringes are introduced, it is always possible to capture the constructive and destructive interferences; the former corresponds to the bright fringes and the latter to the dark fringes. An optical path length change causes a shift of the fringe pattern in a lateral direction at the same frequency as the optical path length change. If the optical path length change is due to the acoustic oscillation of the specimen, the fringes move back and forth transversely to the beam (dither) at the acoustic frequency. The CCD cannot resolve this fast dithering motion. Consequently, the fringe contrast is reduced. If the optical path length change is due to an environmental effect, the fringe shift is most likely slower than the sampling rate and can be resolved as a change in the fringe location by the CCD with the fringe contrast unchanged. A slight angular misalignment changes the fringe spacing, and causes some error in the frequency-domain analysis as will be discussed later. However, the error is much smaller than the simple Michelson method.

The carrier fringe method is especially effective if the fringe data is analyzed in the spatial-frequency domain. The reduction in the fringe contrast due to fast dithering is detected in the Fourier spectrum as a reduction in the height of the main peak at the frequency determined by the fringe spacing associated with $\cos \alpha x$ in Eq. (7). Thus, by forming Fourier spectrum of the optical intensity profile and evaluating the peak height of the spectrum we can evaluate the fringe contrast, and in turn, estimate the oscillation amplitude. The spatial fringe shift due to environmental change in δ_0 does not change the Fourier spectrum as it is not a function of x. An angular misalignment due to environmental disturbance can change the spectrum peak height, but the effect is relatively small (see below).

3. Experimental results and discussion

3.1. Thin film specimens

A pair of platinum-titanium (Pt-Ti) coated silicon (Si) thin film specimens is used in the present experiments. The Si substrate is cut along the [1 0 0] plane and 750 μm in thickness. The Ti layer is coated on the Si substrate and the Pt is coated over the Ti layer. The thickness of the Pt and Ti layers are 100 nm and 10 nm, respectively. In one specimen (the treated specimen) of the pair, the Ti layer is coated after the substrate surface is treated with oxygen-plasma bombardment. This treatment makes the Si surface hydrophilic, and therefore strengthens the Ti-Si bond. In the other specimen (the untreated specimen), the Ti layer is coated without a surface treatment.

3.2. Characterization of Michelson interferometer

(a) Analysis with simple Michelson method

Figure 5 shows the intensity profiles of the reference and signal beams captured by a CCD placed behind the beam splitter. For the measurement of each profile, the other beam is blocked. Thus, they do not include the interference term in Eq. (1). The reference beam is reflected off the mirror (the Y-end mirror in **Figure 2**) and therefore its profile is Gaussian. The signal beam is reflected off the specimen whose surface is not as flat as the mirror. Consequently, its profile is somewhat deformed. When these intensities are subtracted from Eq. (1) for the evaluation of the relative phase in Eq. (2), this causes some part of the interference beam in its cross-sectional area to miss interference. **Figure 6** indicates those non-interfering portion as a dip.
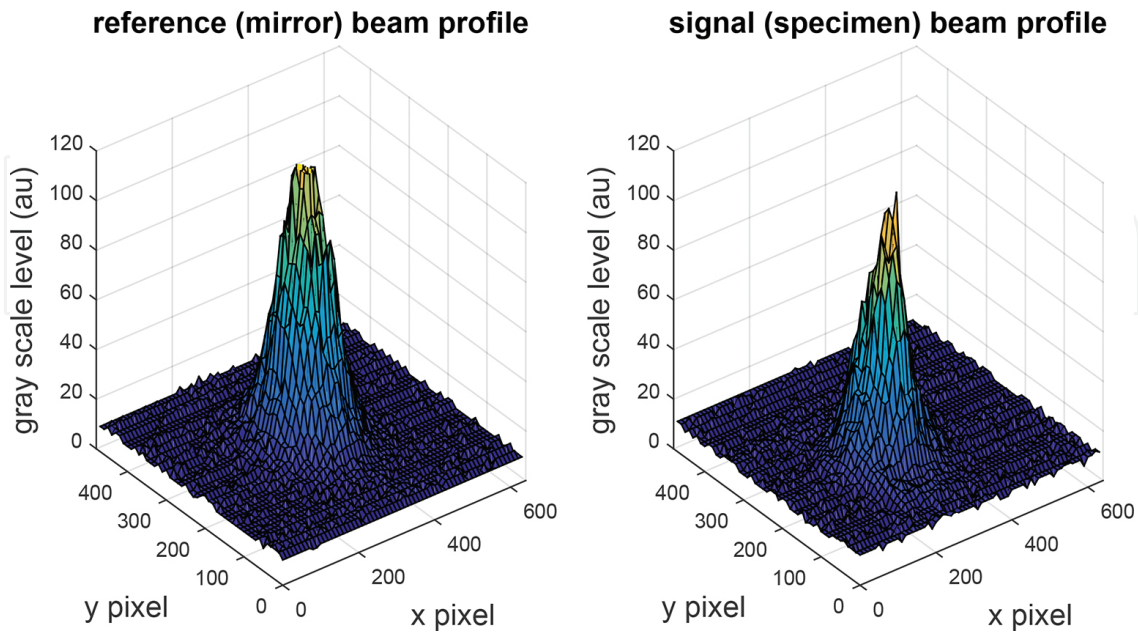
**Figure 5.** Reference and signal beam profiles.
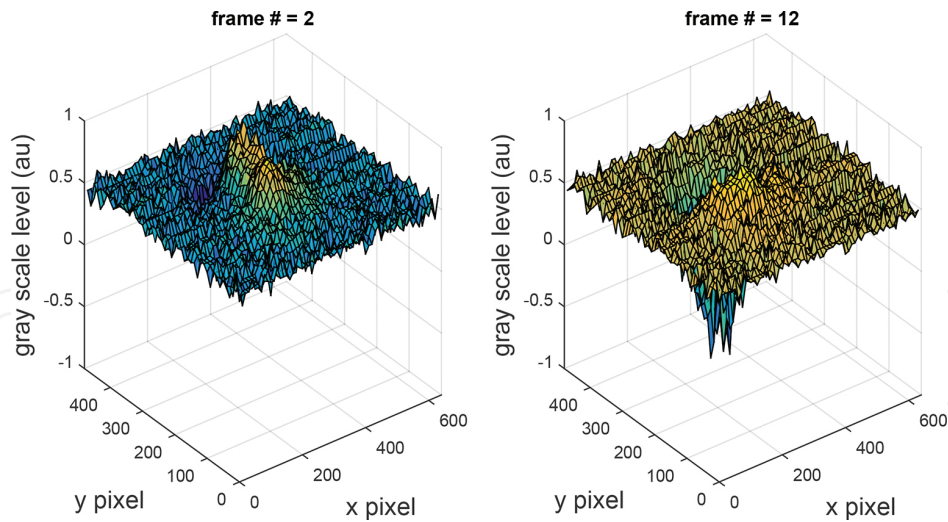
Figure 6. Beam profile of interference term.

The two profiles in **Figure 6** are taken from the same experiment where the specimen is driven by the acoustic transducer under the same condition; the driving frequency and amplitude being the same. The left and right profiles are obviously different. The left profile indicates that the interference term is positive and the left profile indicates that it is more negative. Since the phase change due to the film surface displacement is not large enough to change the sign of Eq. (6) (i.e., it is unlikely that $J_0(\delta)<0$), it is likely that the difference comes from a change in the reference phase difference (δ_0 in Eq. (6)).

Figure 7(a) shows the interference term as a function of time when the acoustic transducer is on and off. Apparently, the fluctuation is significantly higher when the transducer is on. **Figure 7(b)** is the Fourier transform of **Figure 7(a)**. The peak frequency of the disturbance is less than 1 Hz which is lower than the frame rate of the CCD used in the experiment. This indicates that the phase fluctuation affects the approximated expression Eq. (5) when the transducer is on.
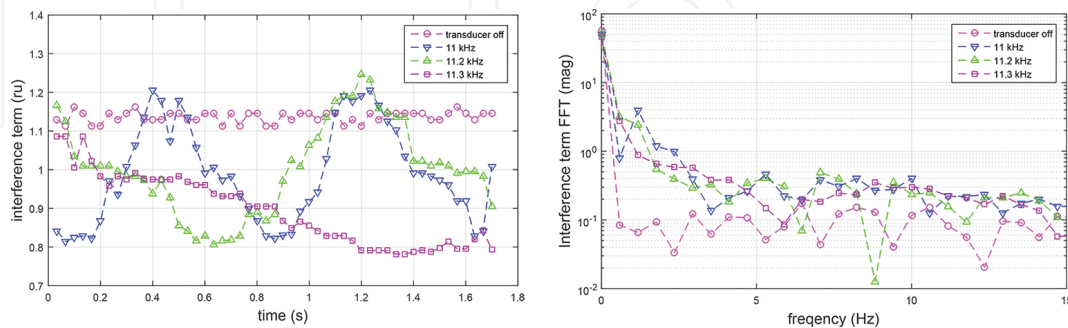
Figure 7. Variation of interference term as a function of time (left) and frequency (right).

It is likely that the temperature rise due to heat emitted from the transducer is one of the causes of the phase fluctuation. An independent temperature measurement indicates that the air

temperature easily rises over 0.1°C within 1 s after the transducer is turned on, and that the temperature fluctuates by ±0.1°C approximately every few minutes. In one set of measurement in which the transducer is turned on and off every 3 min, a total temperature rise of 0.4°C is recorded over a period of 30 min. It is suspected that air convection causes the temperature fluctuation.

It is informative to make a rough estimate of the phase change due to the above temperature change. The optical phase change due to the temperature dependence of the refractive index of air can be expressed as follows.

$$d\phi = 2\pi \frac{l}{\lambda} \frac{\partial n}{\partial T} dT \tag{8}$$

Here λ is the wavelength, l is the path length, n is the refractive index of air and dT is the temperature change. The temperature coefficient $\partial n/\partial T$ of air is -0.87×10^{-6} (1/°C) [8]. The arm length of the interferometer used in this experiment is 10 (cm). The wavelength of the laser used in this study is 632.8 nm. So, the phase change due to a temperature change of ±0.1°C over the round trip in the interferometric arm is 20 (cm)/632.8 (nm) $\times 0.87 \times 10^{-6} \times 0.1 = 2.75\%$ (of the period 2π). Accordingly, the phase error due to the air temperature change of 0.4°C observed over 30 min is $2.75 \times 4 = 11.0\%$ of the period.

The issues of the deformed phase front and the initial phase fluctuation observed in Figures 6 and 7 make it difficult to use Eq. (5) with the total intensity method. In the next section, the carrier fringe method that greatly reduces the influence of the initial phase fluctuation is discussed.

(b) Analysis with carrier fringe method

The fluctuation of the initial phase δ_0 can be evaluated with the carrier fringe method as well. In this case, a change in δ_0 causes a shift in the carrier fringe location. The top row of **Figure 8** shows the spatial shift of carrier fringes at three different driving frequencies. In conducting the measurement at the three driving frequencies, the voltage input to the transducer is adjusted so that the oscillation amplitude of the transducer surface is the same for all the frequencies. It is seen that the shift, i.e., the change in the reference phase δ_0 is rather random, supporting the above speculation that convection of air in the interferometric arm causes the initial phase fluctuation.

The lower row of **Figure 8** is the Fourier spectrum of the spatial intensity variation of the fringe pattern observed at the respective driving frequencies. The first and main spectral peak observed at the spatial frequency of 0.02 (1/pxl) represents the carrier fringe periodicity of the light intensity; $\cos \alpha x$ in Eq. (6) or the fringe pattern (see top of **Figure 9**). The Fourier spectrum is computed from the intensity profile over the horizontal span of 600 pxl (across a horizontal line near row 250 in the fringe image in **Figure 9**). Thus, the minimum frequency is 1/600 (1/pxl). This means that the frequency of 0.02 (1/pxl) corresponds to the 0.02/(1/600) =12th harmonics, or the periodicity of 600/12=50 (pxl). The fringe patterns in **Figure 9** indicate this periodicity.
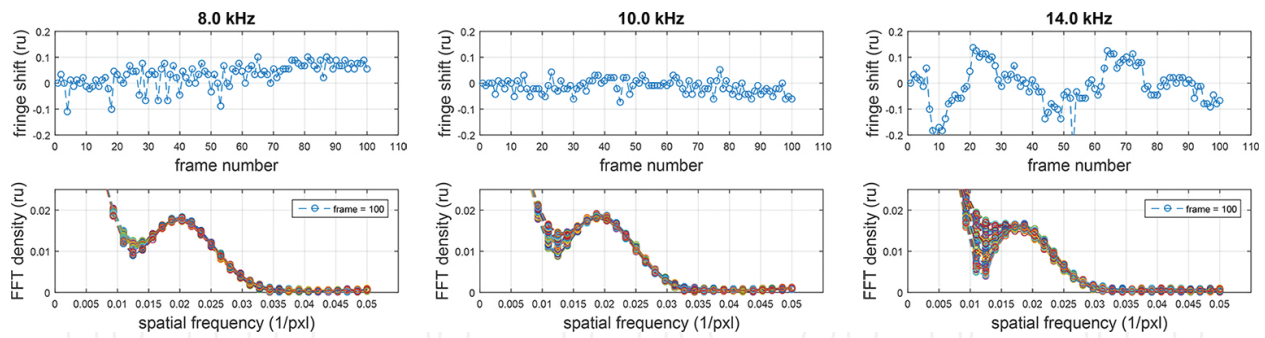
Figure 8. Fluctuation of the initial phase and corresponding change in Fourier spectrum observed with carrier fringe method.
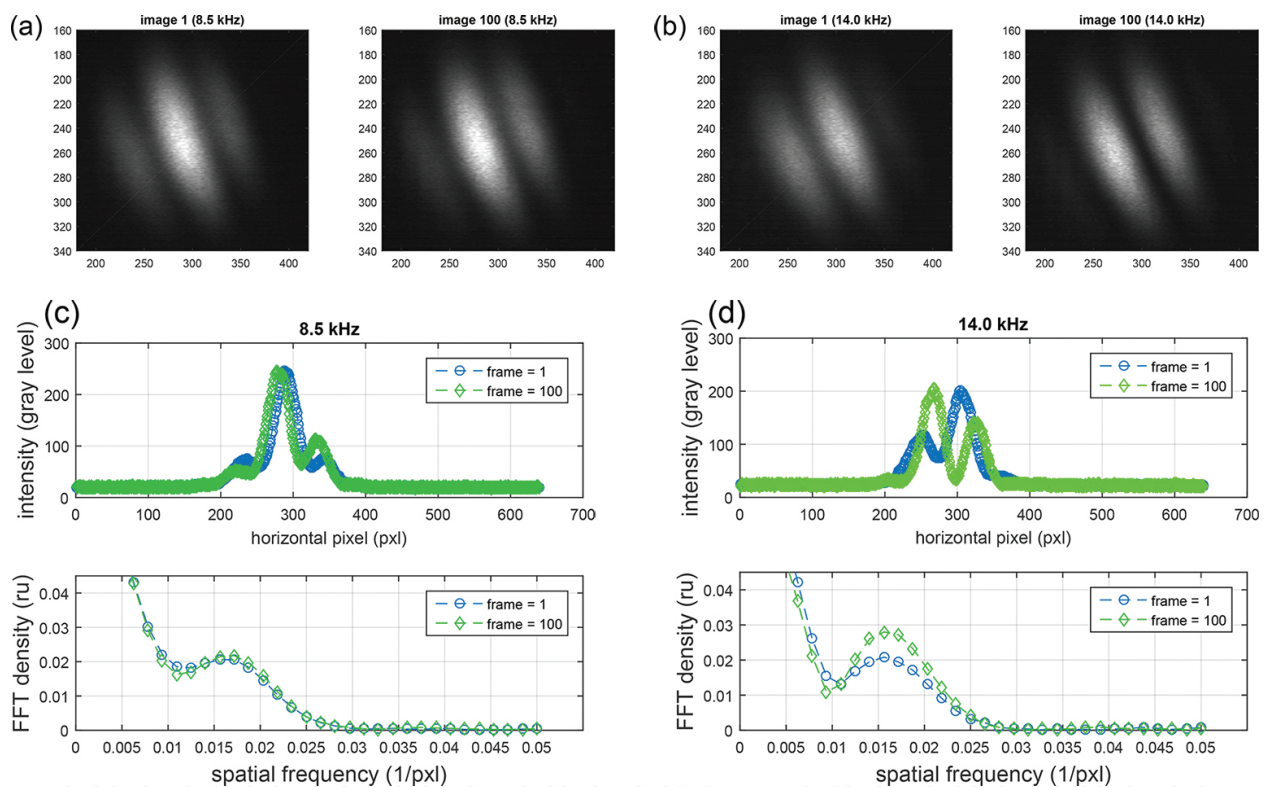
Figure 9. Effect of fringe shift and intensity profile change on Fourier spectrum.

The lower row of **Figure 8** clearly illustrates the advantage of the carrier fringe method. The spectrum plotted for each driving frequency is superposition of 100 frames. Since the CCD frame rate is 30 fps, 100 frames correspond to approximately 3 s in time. Notice that the spectra observed at driving frequency 14.0 KHz show that the spectrum data are scattered in the frequency range left of the peak. This observation indicates that the random variation of the reference phase change is reflected in the low spatial frequency region of the spectrum; as $\cos\delta_0$ changes, the total intensity detected by the CCD fluctuates, and that changes the low spatial frequency component. However, the peak height of the FFT spectrum is unaffected. This is because the peak value corresponds to the spatial dependence $\cos \alpha x$, not $\cos\delta_0$ as a

function of time. Thus, it can be said that the peak height difference comes from the oscillation amplitude δ in Eq. (6). Here, the change in the total intensity depends on the initial phase δ_0; when δ_0 is closer to $\pi/2$ its change is greater as the cosine function has the greatest slope around $\pi/2$ (**Figure 3**). Since the initial phase changes randomly, we have no control over the total intensity.

Figure 9 illustrates the advantage of the carrier fringe method more explicitly. This figure depicts two representative cases observed at driving frequency of 8.5 and 14.0 KHz. For each frequency, the first and last frames of 100 consecutive frames are shown. **Figure 9(a)** and **(b)** shows the fringe images, the upper graphs of **Figure 9(c)** and **(d)** are the spatial intensity profiles over 640 horizontal pixels, and the lower graphs of **Figure 9(c)** and **(d)** are the corresponding Fourier spectra. In the case of 8.5 KHz driving, the fringe pattern shifts approximately by 10 pxl over the 100 frames, but its profile is unchanged. In this case, the peak value of the Fourier spectrum is the same for the first and last frames.

In the case of 14.0 KHz driving, the fringe shift is similar or less than the 8.5 KHz case but the intensity profiles are changed; the fringe image for the first frame (the left image of **Figure 9(b)**) shows that the right bright fringe is stronger than the left bright fringe in intensity whereas the image of the last frame (the right image of **Figure 9(b)**) shows that the left bright fringe is stronger in intensity. The top graph of **Figure 9(d)** indicates the difference in the intensity patterns between the first and last frames more explicitly. In this case, the peak values of the Fourier spectrum for the first and last frames are different.

As indicated above, the fringe shifts are due to the random change in the initial phase. The change in the intensity profile is most likely caused by angular misalignment of the reference and signal beams. These observations indicate that while the carrier fringe method is not affected by fluctuation of the initial phase, the angular misalignment must be suppressed as much as possible to reduce errors.

### 3.3. Frequency domain analysis with carrier fringe method

The consistency of the spectrum peak observed in **Figure 8** indicates that it is possible to evaluate the oscillation amplitude quantitatively. Consider the relation between the input voltage to the acoustic transducer and the oscillation amplitude of the film surface. At a given oscillation frequency, the electric power of the transducer is proportional to the square of the applied (input) voltage, and the mechanical power associated with the elastic motion of the film is proportional to the square of the oscillation amplitude. Thus, the input voltage and the film surface oscillation amplitude are proportional to each other. Under the condition that the oscillation frequency is orders of magnitude higher than the CCD's frame rate, an increase in the oscillation amplitude reduces the fringe contrast (because the CCD cannot follow the fast shift of the fringes). Therefore, it is expected that the blurriness of the fringe pattern increases with the input voltage to the transducer. With the reduction of fringe contrast, the peak value of the Fourier spectrum decreases. Further, by fitting the reduction in the fringe contrast with the use of Eq. (6), it is possible to estimate the oscillation amplitude accurately.

Figure 10 compares fringe contrasts as a function of the input voltage. As expected, the fringe becomes blurrier with the increase in the input voltage. **Figure 11** plots the Fourier spectra obtained at the six voltages (including 0 V) indicated in **Figure 10**. With the increase in the input voltage, the spectrum peak decreases.
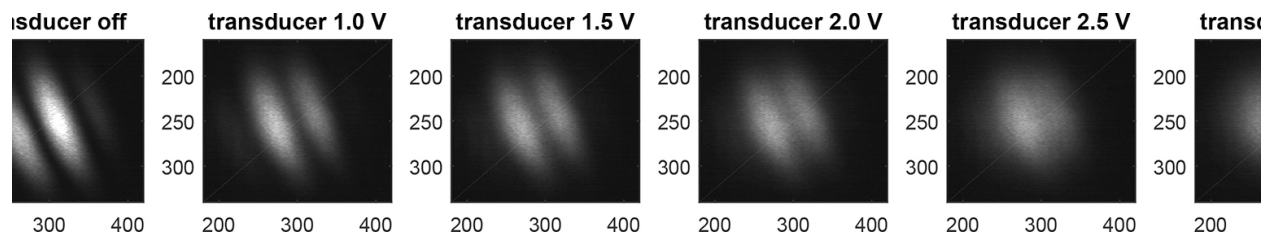

Figure 10. Fringe contrast at various input voltage to transducer.
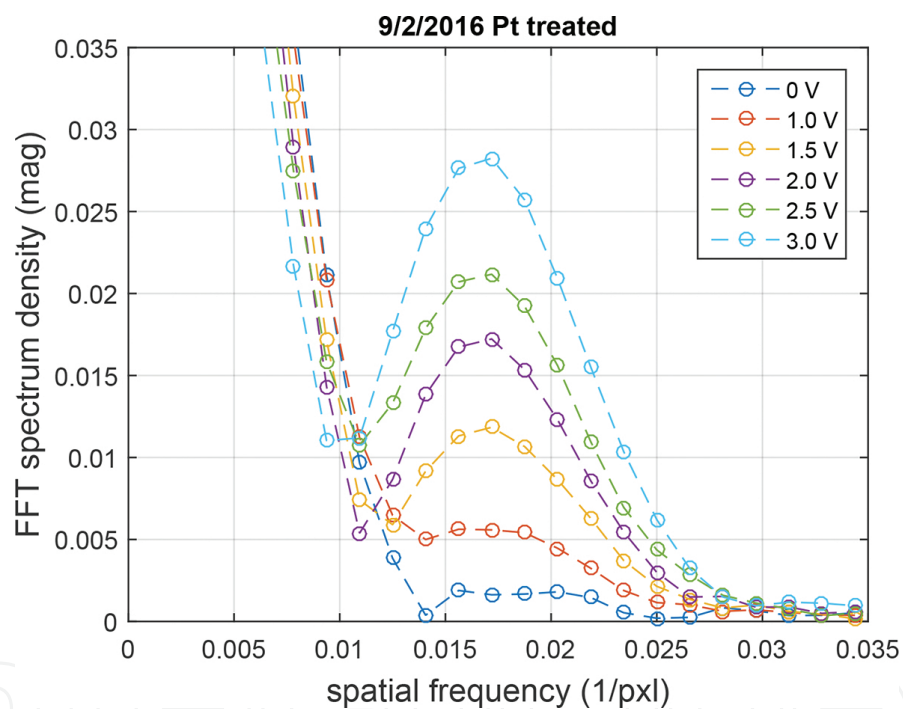

Figure 11. Fourier spectra for six input voltages shown in **Figure 10**.

Based on the proportionality between the input voltage and the oscillation amplitude, it is possible to estimate the oscillation amplitude by fitting the experimental relation between the input voltage and the spectrum peak value to $J_0(\delta)$ (Eq. (5)). When the input voltage is zero hence $\delta = 0$, J_0 takes the maximum value of unity. As the oscillation amplitude increases, $J_0(\delta)$ decreases to the first root at $\delta = 2.4048$. Thus, by evaluating the peak value relative to the case when the transducer is turned off, it is possible to estimate the oscillation amplitude $d = \delta/k$. **Figure 12** plots the peak values shown in **Figure 11** relative to the highest value obtained with the null input voltage using a factor a in $J_0(aV)$ as the fitting parameter. Here V denotes the input voltage. The measured spectrum peak values fit to the Bessel function reasonably well.
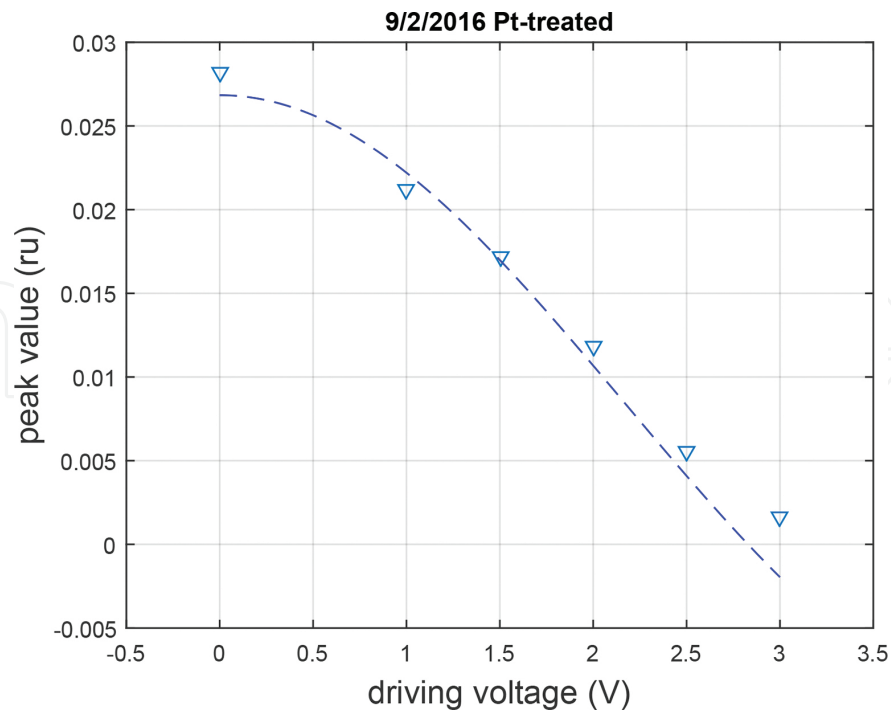
Figure 12. Spectrum peak value as a function of input voltage to transducer.
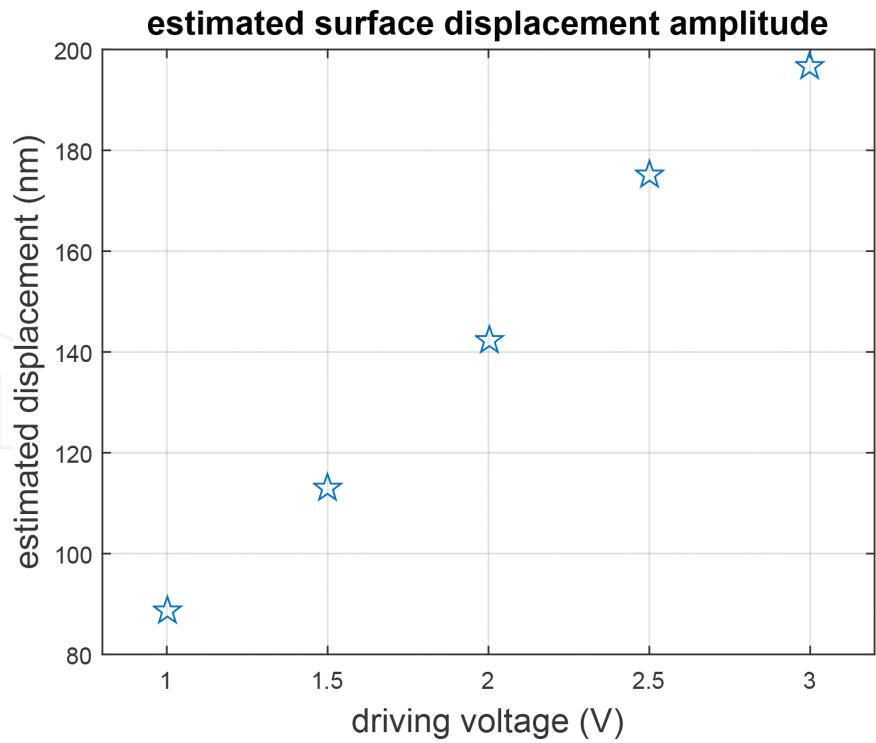

Figure 13. Oscillation amplitude estimated for each voltage input.

Now that the Bessel function-like behavior of the spectrum peaks is confirmed, the value of δ can be estimated from the spectrum peak value obtained for each input voltage relative to the peak value obtained with the transducer turned off (zero input voltage). Subsequently, the oscillation amplitude can be found from $d = \delta/k$. **Figure 13** plots the value of d found in this fashion.

3.4. Driving frequency sweep

By repeating the same measurement as the lower row of **Figure 8**, it is possible to find out the frequency dependence of the film surface. As is the case of **Figure 8**, the input voltage to the acoustic transducer is adjusted so that the oscillation amplitude of the transducer surface is the same for all the driving frequencies tested. **Figure 14** shows the result of such a series of measurement for a driving frequency range of 8–14.5 KHz. Here, the vertical axis is the value of the Fourier spectrum peak obtained from the intensity profile across the fringe pattern averaged over five rows near the vertical center of the fringe images. In accordance with the argument made above, the higher the peak, the smaller the film surface oscillation. Since the transducer surface has the same oscillation amplitude for all the driving frequencies, the frequency dependence of the film surface oscillation observed in this figure represents the transducer surface to the film surface transfer function. Since the transfer function of the substrate and film materials themselves are considered to be unity
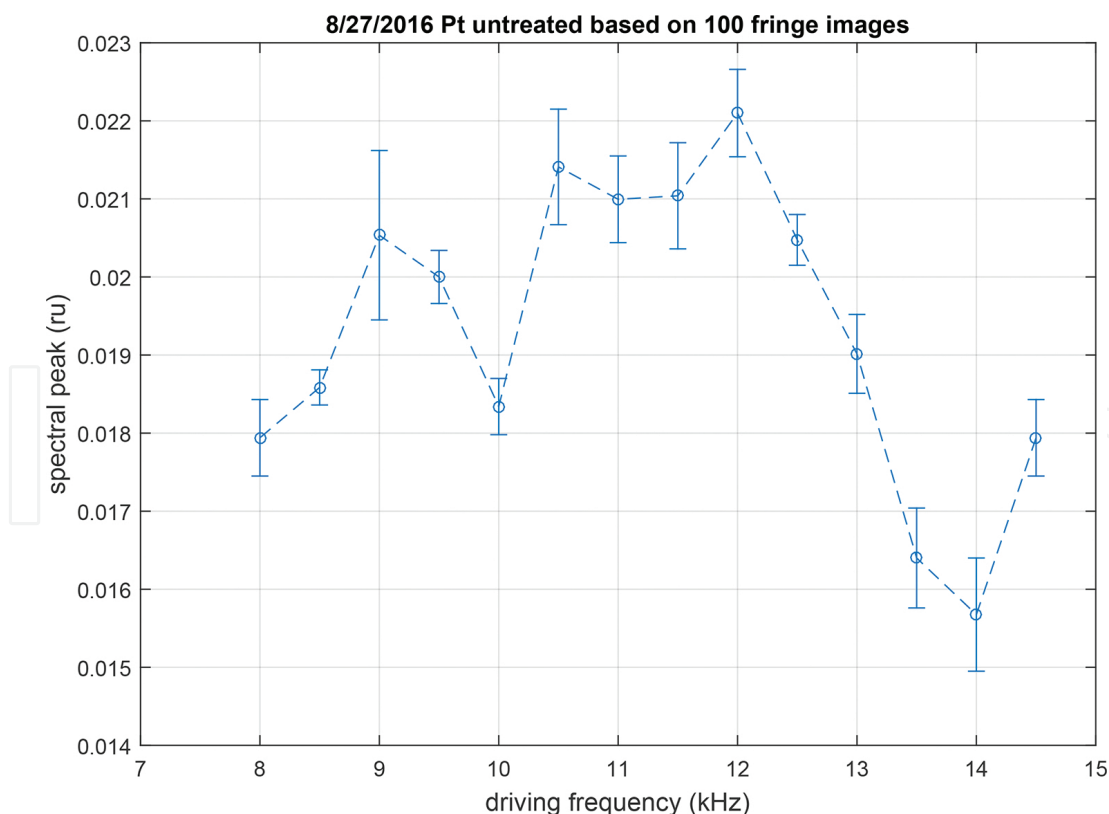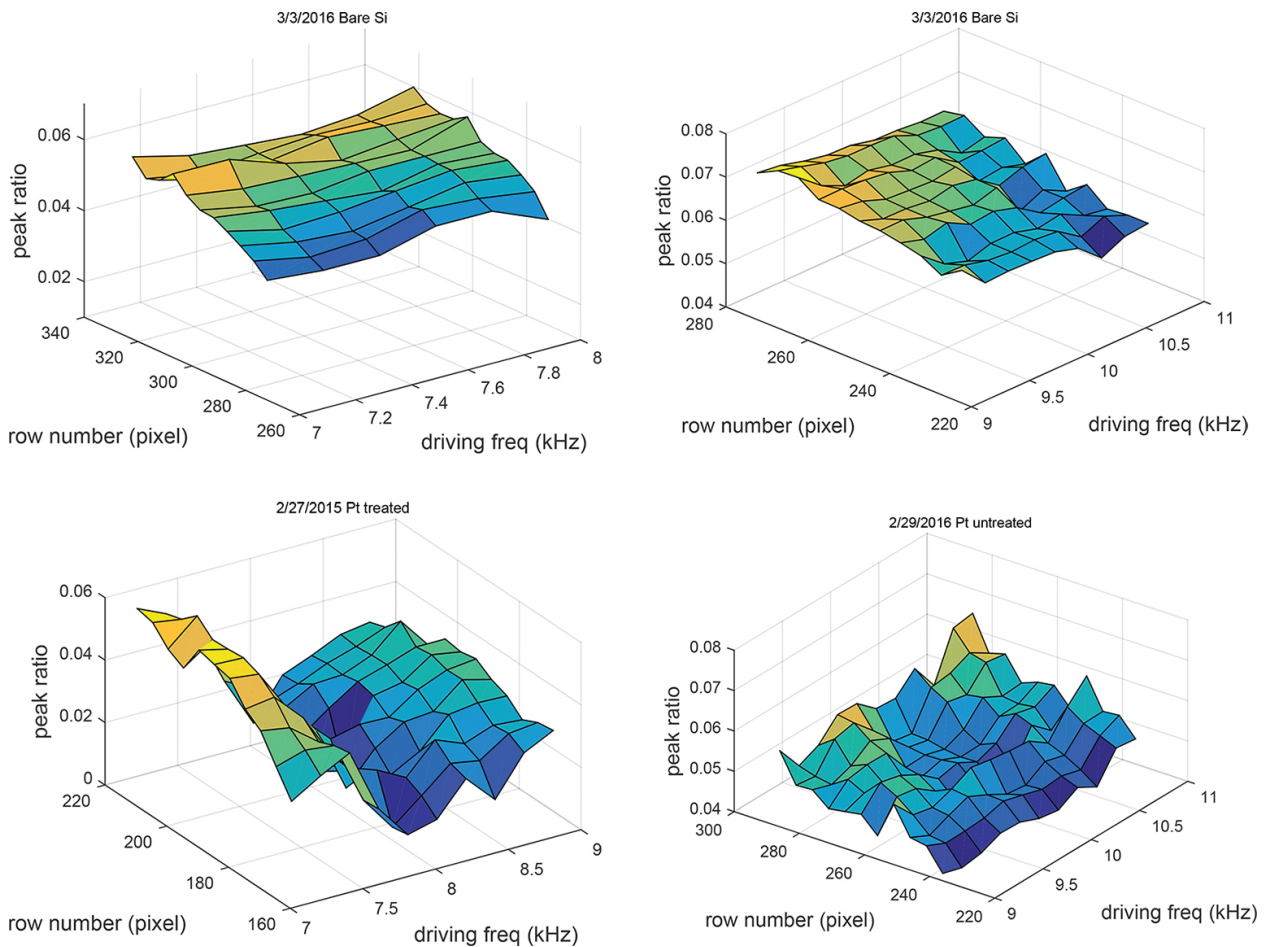

Figure 14. Driving frequency sweep of Fourier spectrum peak value.

in this frequency range, the transfer function represents the elastic property of the film-substrate interface. The lower the spectrum peak the greater the oscillation on the film surface, which can be interpreted as the greater oscillation of the interface.

The transfer function shown in **Figure 14** is obtained for five rows near the vertical center of the fringe image. By repeating the same procedure for other rows, it is possible to draw a map of the transfer function. **Figure 15** shows a three-dimensional map obtained in this fashion for four specimens; the untreated, treated, and bare silicon specimens. Here one horizontal axis is the row number and the other horizontal axis is the driving frequency. The top two plots are the cases when silicon substrates only are used (called the bare silicon specimens), and the bottom two plots are cases when the treated and untreated specimens are used. The treated and untreated specimens are attached to two different acoustic transducers. To eliminate the effect associated with the use of the different transducer, one bare silicon specimen is attached to the same transducer as the treated specimen and the other bare silicon specimen is attached to the other transducer used for the untreated specimen.

Figure 15. Fourier spectrum peak for several rows as a function of driving frequency.

The two plots for the bare silicon specimens appear to be flat, indicating that the bare silicon specimens do not have clear frequency dependence in the oscillation. On the other hand, the

treated and untreated specimens show frequency dependences. As mentioned above, the frequency dependence represents the elastic characteristics of the substrate-film interface.

It is interesting to note that the untreated specimen shows a crater-like pattern around row 250 through 280 near driving frequency of 10 KHz. It is possible to interpret this pattern as representing the so-called blister effect [9–11]; the interface has a weakly adhered spot where the film experiences membrane-like oscillation when the specimen is driven. The treated specimen does not show a crater-like pattern. Instead, there is a valley running through all rows around the driving frequency of 8 KHz. We observed similar patterns in the treated and untreated specimens for a number of times. It is possible that the precoating surface treatment makes the adhesion more uniform so that the chances of the specimen having blisters is lower. These observations particularly interest us because there is no established technique to evaluate the blister effect non-destructively.

4. Conclusion

An optical interferometric method to characterize the elastic behavior of the interface of thin-film systems is discussed. The thin-film specimen is configured as one of the end-mirrors of a Michelson interferometer with the film side facing the beam splitter. The specimen is oscillated sinusoidally with an acoustic transducer. The harmonic response of the film surface to the acoustic oscillation is detected as relative optical phase difference between the two interferometric arms. An algorithm to estimate the amplitude of the film surface oscillation from the relative optical phase measurement is discussed.

Environmental noise that compromises the relative phase measurement is analyzed. The use of a carrier fringe system in conjunction with analysis in the spatial frequency domain is proposed as a method to reduce the influence of environmental noise is discussed. Under some conditions, the effectiveness of the proposed method is demonstrated with experiment.

A sample set of data obtained with Pt-Ti-Si thin-film system is presented. The three-dimensional mapping of the adhesion strength obtained with the carrier fringe method indicates some behavior of the film surface that can be interpreted as representing the so-called blister effect. It is interesting to note that the blister-like behaviors observed in the surface-treated and non-treated specimen are different from each other. This observation is of particular interest to us as non-destructive evaluation of the blister effect is not easy. More investigation is under way.

Acknowledgements

Author details

Sanichiro Yoshida[1*], David R. Didie[1], Jong-Sung Kim[2] and Ik-Keun Park[2]

*Address all correspondence to: syoshida@selu.edu

1 Department of Chemistry and Physics, Southeastern Louisiana University, Hammond, Louisiana, USA

2 Department of Mechanical and Automotive Engineering, Seoul National University of Science and Technology, Nowon-gu, Seoul, South Korea

References

[1] Lemons RA, Quate CF: Acoustic microscopy. In: Mason WP, Thurston RN, editors. Physical Acoustics. London: Academic Press; 1979; Vol. XIV, pp. 1–92.

[2] Weglein RD: Acoustic microscopy applied to SAW dispersion and film thickness measurement. IEEE. Trans. Sonics. 1980; 27: 82–86.

[3] Atalar A: An angular-spectrum approach to contrast in reflection acoustic microscopy. J. Appl. Phys. 1978; 49: 1530–1539.

[4] Atalar A: A physical model for acoustic signatures. J. Appl. Phys. 1979; 50: 8237–8239.

[5] Telschow KL, Deason VA, Cottle DL, Larson JD: III: Full-field imaging of gigahertz film bulk acoustic random motion. IEEE. Trans. Ultrason. 2003; 94: 79–88.

[6] Yoshida S, Didie DR, Didie D, Sasaki T, Park HS, Park IK, Gurney D: Opto-acoustic method for the characterization of thin-film adhesion. Appl. Sci. 2016; 6: doi:10.3390/app6060163.

[7] Sciammarella CA, Sciammarella FM: Experimental Mechanics of Solids. Hoboken: Wiley; 2012. ISBN-10: 0470689536.

[8] Effect of Temperature on Refractive Index (dn/dt). Available from: http://www.ohara-gmbh.com/e/katalog/tinfo_2_4.html [Accessed on 2016-09-11].

[9] Bedrossian J, Kohn RV: Blister patterns and energy minimization in compressed thin films on compliant substrates. Commun. Pure Appl. Math. 2015; 68: 472–510.

[10] Dennenberg H: Measurement of adhesion by a blister method. J. Appl. Polym. Sci. 1961; 5: 125–134.

[11] Volinsky AA, Moody NR, Gerberich WW: Interfacial toughness measurements for thin films on substrates. Act Mater. 2002; 50: 441–466.